AIAA SciTech Forum
23-27 January 2023, National Harbor, MD & Online
AIAA SCITECH 2023 Forum

10.2514/6.2023-0263

A Brief Review of Electrospray Propulsion Diagnostics

Christopher T. Lyne*, Miron F. Liu**, and Joshua L. Rovey†
University of Illinois at Urbana-Champaign, Urbana, IL, 61801, United States

We review common experimental techniques used in electrospray propulsion, including the direct measurement of thrust and propellant flow rate, and the measurement of plume properties such as mass flux, mass-to-charge distribution, and stopping potential distribution. We also discuss more complex diagnostics, such as using retarding potential and mass spectrometry in tandem. Plume diagnostics are summarized in a table for convenience. Next, we discuss how thrust and propellant flow rate can be estimated from plume data. Citing recent examples from the literature, we show that indirect 'measurements' of thrust and flow rate generally agree with direct measurements within ~15% for capillary electrospray thrusters. For passively fed thrusters, plume-based estimates of thrust are reasonably accurate, but plume-based estimates of propellant flow rate are not reliable, differing from direct measurements by a factor of ~2.5 in one prominent study. These conclusions highlight the need for direct measurements, when possible, and for continued investigation of mass loss mechanisms in passively fed electrospray thrusters.

Nomenclature

ϕ_{SP}	Stopping Potential	Kinetic energy per unit charge, expressed in Volts
ζ	Mass-to-charge ratio	Inverse of specific charge
j	Current density	Charge passing through a unit area per time (flux)
j_m	Mass flux	Mass passing through a unit area per time
j_p	Momentum flux	Momentum passing through a unit area per time
v_z	Axial velocity	
T	Thrust	
$\dot{m}$	Mass flow rate	
MS	Mass Spectrometry	Method for measuring specific charge in a plume
ToF, ToF-MS	Time of Flight	Mass spectrometry method
RP	Retarding Potential	Method for measuring ϕ_{SP}
RPA	Retarding Potential Analyzer	Instrument for measuring ϕ_{SP}
RP/MS	RPA and MS in tandem	Tandem method used to measure ϕ_{SP} and ζ
EMI-Im	An ionic liquid propellant with the chemical name 1-ethyl-3-methylimidazolium bis(triflouromethylsulfonyl)amide	
EMI-BF_4	An ionic liquid propellant with the chemical name 1-Ethyl-3-methylimidazolium tetrafluoroborate	

I. Introduction

Electrospray propulsion is a type of electric propulsion in which ions, ion clusters, and charged droplets are extracted directly from the surface of a liquid propellant and accelerated to produce thrust. Electrospray emission occurs at a small scale, with each emission site emitting nanograms to micrograms of propellant each second to produce micronewtons or less of thrust. This quality makes electrospray easy to miniaturize and to scale (in theory) but makes it more challenging to study. For example, characterizing a new thruster prototype may require measuring thrust at the ~10 μN level, and measuring flow rates of single nanoliters per second. Since making direct measurements can be difficult and expensive, the thrust and flow rate are often indirectly 'measured' (i.e., estimated) using plume diagnostics. In principle this can be done by integrating the momentum flux and mass flux, respectively, over a surface enclosing the plume. However, when indirect 'measurements' are compared with direct measurements, they don't necessarily prove to be accurate.

This paper reviews direct and indirect measurement methods for electrospray propulsion, including common measurement techniques, some of their nuances and shortcomings, and their use in estimating thrust and flow rate. Section III explores the theory of indirect measurement and cites examples from the literature where direct and indirect methods have been compared. From that review, it is clear that plume-based methods can provide reasonable estimates for thrust and flow rate, especially for capillary electrosprays. However, for passively fed electrospray thrusters, plume-based methods appear to underestimate the flow rate by as much as 60% [1]. Practical recommendations for making accurate indirect measurements are presented in section III.C.

II. Electrospray Measurements

The experimental study of electrospray propulsion generally relies on measuring several key metrics. At the system level, experimentalists are interested in the thrust and specific impulse of a thruster, at what voltage it operates, and what its power requirements are. The power consumption can be found by measuring the relevant applied voltages and currents (section II.A). Thrust is usually measured directly, as described in section II.B. Propellant flow rate can be directly measured in a variety of ways, depending on the type of electrospray thruster (section II.C).

In addition to these system-level measurements, plume measurements are often made for two primary reasons. First, measurements of plume properties yield some of the most significant scientific information about electrospray. For example, measurements in capillary electrospray plumes have led to a detailed understanding of the physics of cone-jet electrosprays [2]. Section II.D describes an array of plume diagnostics used in electrospray propulsion. The second main reason plume diagnostics are used is provide indirect estimates of the thrust and propellant flow rate without needing to measure them directly. Section III discusses methods for indirect measurements and examines their accuracy by comparing direct and indirect thrust and flow rate measurements from the literature.

II.A. Voltage and Current

Some of the most basic measurements made when testing an electrospray thruster are the voltages and currents to the emitter and extractor. This section discusses voltage measurement using simple voltage dividers or high voltage probes, and current measurement using isolation amplifiers.

II.A.1. Voltage Measurement

Electrospray thrusters often operate at voltages around 1 kV to 3 kV. Clearly, kilovolt-level voltages are too high to be measured directly with most data acquisition (DAQ) systems. For example, the DAQ used in this work is a National Instruments USB-6210, which has a maximum input voltage of ±10 V. Laboratory power supplies often provide a 'voltage monitor', which outputs a signal that is proportional to the high voltage output. If available, this is often the best option for measuring the voltage applied to the emitter or extractor. If monitoring voltage using a built-in 'voltage monitor' is not feasible, a commercial high voltage probe (e.g., Tektronix P6015A) or a simple resistive voltage divider can be used to reduce the magnitude of high voltage signals. For example, a resistive divider made from a 10 MΩ and a 10 kΩ resistor can reduce the measured

voltage by approximately 1000:1. Whatever method is used, be mindful of any 'parasitic current' caused by the voltage measurement and any error it may introduce into current measurements.

II.A.2. Current Measurement

Measuring current to an electrode at ground potential is simple. One can use a commercial ammeter or a simple circuit such as a current shunt or transimpedance amplifier. However, be mindful that the emitter may arc to the extractor and cause a surge in current. Appropriate protection measures should be taken so that these surges do not damage the measurement equipment. For example, Lyne et al. (2022) used a Keithley 6485 Picoammeter for extractor current measurements [3]. They used an overload protection circuit given in figure I-17 of the ammeter's instruction manual for surge protection. The circuit consists of a series limiting resistor followed by two antiparallel diodes that clamp the voltage at the input of the protected device. A similar protection circuit can be used with other ammeters or current measurement circuits by selecting an appropriate series resistance according to the applied voltages and the limits of the measurement device.

Measuring current to high-voltage electrodes is more challenging. Fundamentally, this is because the *common-mode* voltage of the high voltage electrode is outside the input range of most DAQ equipment. Consider a current shunt, i.e., a resistor that is used to convert current to a measurable voltage difference across the resistor. Suppose that a simple current shunt is used to measure emitter current in an electrospray experiment where the emitter potential is +2 kV, and the extractor is grounded. If the shunt is 100 kΩ and the emitter current is 1 μA, the differential voltage is $\Delta V = 100\ mV$, which is easily measurable with most DAQ devices. However, the voltage on either side of that shunt is 2000 V and 1999.9 V, and most DAQ devices would be damaged by measuring voltages that high. In this case, electrical *isolation* is needed so that the common mode voltage can be blocked while the differential voltage (the 100 mV across the shunt) is passed through to the DAQ. High voltage oscilloscope probes are available that provide isolated measurements (e.g., Tektronix P5200A), but they are relatively expensive and may not meet the voltage requirements of a given application. Instead, commercially available *isolation amplifiers* are often used. Isolation amplifiers work by measuring a differential voltage at their input, then communicating that input voltage across a barrier that electrically isolates the input and output sides of the amplifier. The output signal is proportional to the differential input voltage but is near ground potential so that it can be measured by a standard DAQ system. For example, Lyne et al. (2022) uses an AMC1311 isolation amplifier from Texas Instruments to measure emitter current. They put a current shunt in series between the emitter power supply and the emitter. The differential voltage across the shunt was connected to the amplifier inputs, and the amplifier output signal was measured by a standard DAQ system. They also added overcurrent protection to their circuit using Zener diodes to prevent damage to the isolation amplifier. The AMC1311 is a good candidate for use in electrospray experiments because of its high working voltage limit ($\leq 2120\ V\ DC$), low input bias current (3.5 nA typical), and the availability of an 'evaluation module' (AMC1311EVM) to help with circuit prototyping.

II.B. Thrust

Thrust measurement for electrospray propulsion is often challenging due to the low thrust levels. Single electrospray emitters produce thrust on the order of 0.1 μN for ion sources [1,4] and 1 μN for mixed ion-droplet sources [5]. For comparison, a single grain of rice has a mass of approximately 25 mg, and weighs about 250 μN. So, the thrust from a single electrospray emitter is two or three orders of magnitude lower than the weight of a single grain of rice. Furthermore, a resolution of significantly less than the measured thrust value is needed to precisely quantify the thrust. This section discusses common methods used to make these challenging measurements.

Practical applications of electrospray for in-space propulsion typically require multi-emitter thrusters to be used to reach an acceptable thrust level. Multiplexing emitters is also a practical way to make direct thrust measurements easier. Examples of instruments used for thrust measurement on multi-emitter electrospray thrusters include torsional thrust stands [5–8] and mass balances adapted for in-vacuum use [4,9]. For example, Gilpin et al. (2022) described a dual-axis torsional thrust stand used for simultaneous thrust and mass flow measurements with resolutions of ±0.2 μN and ±0.04 mg, respectively [6]. They used the instrument to take

thrust and mass loss measurements of an AFET-2 porous electrospray thruster operating with the ionic liquid EMI-BF_4. The thruster has 576 emitters machined from porous borosilicate glass. It was operated in current-control mode at 200 μA and produced a thrust of about 14 μN. While the torsional thrust stand had sufficient resolution to quantify the thrust, thermal drift introduced significant error into the measurements. Their results show that thermal drift leads to 7 μN of thrust error after 5 hours of operation, and 26 μN of error after 48 hours.

Others have adapted commercially available analytical mass balances to measure thrust [4,9] For example, Borja De Saavedra et al. (2022) adapted a Mettler Toledo AX504 analytical balance to operate in vacuum for thrust measurements [4]. The balance has a resolution of 0.1 mg (1 μN) and can support a maximum load of 510 g. They used the balance to characterize a passively fed, externally wetted thruster spraying EMI-Im and producing a thrust of 5 μN to 25 μN. The thruster was placed on the balance in vacuum and its plume was directed upward. Thrust was then recorded as the difference in force measured with the thruster firing and not firing. Their results suggest good repeatability for thrust measurement, on the order of a few μN. Although they did not present results for thruster mass loss over time, this configuration could also be used to provide mass flow measurements to enable the calculation of specific impulse.

While conventional thrust stands (e.g., torsional pendulum) are the most commonly used devices for direct thrust measurement in the electrospray propulsion literature, some 'less direct' methods have been developed. For example, the MIT Space Propulsion Laboratory uses a magnetically levitated thrust stand to infer thrust from angular displacement of the levitated platform. Jia-Richards et al. (2022) used this thrust stand to measure the thrust from a pair of electrospray thrusters operating in opposite polarities. There are two unique features of the maglev thrust stand that separate it from the others discussed here. First, in principle, the measurable thrust level has no lower limit. Because the thrust is inferred from the angular displacement over time, even miniscule thrusts can be measured. In practice, imperfections in the magnetic levitation system cause unwanted oscillations that put a lower limit on the thrust that can be reliably measured. The second unique feature is that the thrusters are electrically isolated from their surroundings. In most lab tests, thrusters are powered by laboratory power supplies, which prevent the buildup of excess charge on the thruster. In contrast, the maglev thrust stand is electrically isolated from the surroundings, making it an ideal test facility for studying spacecraft charging (e.g., [10]).

Another category of 'less direct' instruments for thrust measurement is impingement-type thrust stands, which rely on the fact that the momentum flux imparted to the electrospray plume is equal and opposite to the reaction force on the thruster (i.e., the thrust). These devices measure thrust by 'catching' the thruster plume by allowing it to impinge on a surface. The resulting force on that surface is measured to infer the thrust. For example, Chakraborty et al. (2015) developed an impingement-type thrust stand with a resolution of 10 nN for measuring the thrust of single electrospray emitters [11]. Their device uses a lightweight impingement plate that the plume impacts. The plate transfers the force to a commercial force sensor, which has a resolution of 5 nN measured at 10 Hz. Thrust is measured by interrupting the electrospray plume and recording the change in force on the impingement plate. The signal-to-noise ratio is improved by interrupting the plume at a well-defined frequency and using a lock-in amplifier to amplify the signal measured at that frequency. The narrow bandwidth of the lock-in amplifier reduces the effect of noise from other sources, such as vibration due to pumps. The thrust stand presented by Chakraborty et al. is able to achieve a resolution that is nearly two orders of magnitude lower than the torsional thrust stands described in the previous paragraphs. This increase in sensitivity is possible because the design separates the weight of the thruster from the force measurement. Torsional thrust stands, and those based on mass balances, must support the weight of the thruster in addition to measuring the thrust produced. Since the thrust-to-weight ratio of an electrospray thruster might be 10^4, small errors due to imperfect leveling of the thrust stand can become important. Similarly, the bearings and other hardware that are required to support the thruster weight (as well as the weight of the torsional pendulum itself) can contribute significantly to error in thrust measurement.

In the previous paragraphs, we've seen that the low thrust levels typical of electrospray thrusters can make direct measurement of thrust difficult. Often achieving adequate resolution requires complex designs and/or expensive equipment. For these reasons, making indirect *estimates* of thrust has become a popular approach

for studying prototype electrospray sources. Although there is no substitute for the reliability of direct thrust measurements, indirect estimates based on plume measurements are often worthwhile. We will further discuss indirect methods for thrust estimation in section III.

II.C. Mass Flow

The second quantity of primary interest to the electrospray experimentalist is the propellant flow rate. Measuring the propellant flow rate is necessary to calculate the specific impulse of the thruster, a key figure of merit. For capillary electrosprays, one popular method is to seed a gas bubble into the capillary feed tubing and measure its velocity with the help of an optical microscope (e.g., [3]). Commonly, propellant feed systems for capillary sources are based on controlling the feed pressure at the inlet of the propellant feed tubing. Many researchers use bubble tracking to measure propellant flow rate as a function of feed pressure, which should be linear according to Poiseuille flow. While this method is very common, it is far from infallible. For example, if the hydraulic resistance of the feed tubing changes, so does the relationship between feed pressure and flow rate. This could easily happen due to a partial or full clog of the tubing. Another source of error is the temperature-dependent viscosity of the propellant, which may vary considerably near room temperature. Another possibility, which we have observed ourselves but have not read in the literature, is that the flow rate in the tubing where the seeded bubble is can differ from the flow rate that is arriving at the emitter tip due to the accumulation of gas bubbles downstream of the flow measurement section. Those gas bubbles could result from repeatedly seeding bubbles for tracking, or from volatile components dissolved in the propellant, especially since many of the popular ionic liquid propellants readily absorb water from the atmosphere.

Another option for measuring propellant flow rate in a capillary electrospray experiment is to measure the differential pressure across a section of tubing. For example, Smith et al. (2006) built a flow meter based on differential pressure measurements across a section of tubing [12]. Their flow meter achieved a resolution of 0.03 nL/s and an absolute accuracy of 0.3 nL/s, which is considerably lower than commercially available flow meters. They used their flow meter to investigate the effect of applied voltage on the propellant flow rate in pressure fed feed systems. They found that, for a nominal flow rate of 4 nL/s and a fixed feed pressure, the fractional variation in flow rate was approximately equal to the fractional variation in applied voltage. i.e., A 25% increase in voltage led to a ~25% increase in flow rate at a fixed feed pressure. This finding is in direct conflict with the common assumption that the Hagen-Poiseuille equation can be used to relate flow rate and feed pressure. That is, the effect of applied voltage on flow rate is often ignored. At the very least, their findings suggest that pressure – flow rate calibration (e.g., using bubble tracking) should be done while electrospraying at the nominal emitter voltage. The flow meter used by Smith et al. gives them real time flow rate data while electrospraying, but ultimately this method may yield an incorrect flow rate if the tubing section between the two pressure sensors becomes clogged.

The measurement of propellant flow rate is more challenging for passively fed electrospray sources such as porous or externally wetted electrospray thrusters. These sources do not generally use a tube to feed propellant to the emitter. Rather, propellant is stored in a reservoir in the thruster, and passively wicks to the emitter tips by capillary action. Because the movement of propellant inside the thruster is not directly observable, experimentalists typically rely on mass change for direct flow rate measurements. Mass loss measurements have been made using commercial mass balances adapted for use in vacuum [7] and with custom-made mass balances [6]. For example, Gilpin et al. (2022) used a dual axis torsional thrust stand to simultaneously measure thrust and mass loss while testing a porous electrospray thruster [6]. Over a 16 hour test, they measured a total mass loss of 50.7 mg, which corresponds to an average flow rate of 0.053 mg/min. The torsional mass balance they use has a resolution of 0.04 mg, so it takes about 45 seconds for the mass to change by an amount equal to the resolution of the mass measurement. Also note that Gilpin et al. used the AFET-2 porous electrospray thruster, which has 576 active emitters, so the flow rate they measured per emitter is approximately 1.5 ng/s. Clearly, the flow rate for a single porous electrospray emitter is nearly impossible to measure directly in a reasonable amount of time. Thankfully, techniques have been developed to estimate flow rate from plume data. Section III will discuss these indirect measurements. However, section III.B.3 shows that indirect flow rate estimates for passively fed thrusters are not reliable, sometimes differing from direct measurements by a factor of ~2.5.

II.D. Plume Properties

In addition to quantifying propulsive performance by measuring thrust and propellant flow rate, experimentalists need to understand the characteristics of the electrospray plume. Reasons for studying the plume range from the practical, such as understanding how electrospray plumes can contaminate spacecraft, to the scientific, such as measuring the rates of ion cluster fragmentation. Ultimately, understanding the plume is a key piece of understanding the fundamentals of electrospray and may lead to advances in areas such as computer modeling, design, and lifetime.

This section is organized by the various quantities to be measured in an electrospray plume. The most basic are the fluxes of charge and mass throughout the plume (sections II.D.1 and II.D.2, respectively). Also relevant are the mass-to-charge (II.D.4) and kinetic energy-per-charge (II.D.3), which we refer to as the *stopping potential* ϕ_{SP}. At each point in the plume, there is a mass-to-charge distribution (sometimes called a *mass spectrum*) and a *stopping* potential distribution. While these measurements are often reported independently, plume diagnostics can be used in tandem to quantify these distributions more fully, as discussed in section II.D.5. Section II.D.6 discusses other measurement techniques that are less common but still relevant to our discussion of electrospray propulsion diagnostics. Finally, section II.D.7 summarizes the various plume measurements and methods.

II.D.1. Current Density

Plume current is perhaps the simplest plume property to measure. Often, plume current is measured using a Faraday cup, which simply 'catches' the charge that impinges on the metallic cup-shaped collector so the resulting current can be measured. Plume current density can be calculated by dividing the measured current by the effective area of the Faraday cup. While plume current measurements using a Faraday cup are simple, high-energy particles impacting the cup collector can cause secondary species to be emitted from the surface. Recent studies have shown that a variety of secondary species are emitted, including those with a net charge, and can cause significant error in the measurement of impinging plume current [13,14]. For more information about secondary species emission, see section II.D.6.

II.D.2. Mass Flux

The second plume property in our discussion is the plume mass flux (j_m), which refers to the mass flow rate per unit area or solid angle in the plume. Electrospray plumes can contain a diverse mix of particles including polyatomic ions, clusters of ions, nanodroplets, and neutral species resulting from the fragmentation of larger, charged species. For example, an ion cluster containing two cations and one anion (called a *dimer*) can spontaneously fragment into a single cation (a *monomer*) and a neutral cation-anion pair. The presence of these neutral species in addition to charged species makes the measurement of plume mass flux particularly challenging.

A common method for measuring plume mass flux in electrospray plumes is to use a quartz crystal microbalance (QCM). A QCM is a diagnostic frequently used to monitor the thickness of thin films as they are being deposited. The QCM uses a quartz crystal, which has a distinct and well-known resonant frequency, much like quartz oscillators in clocks. In a QCM, mass impinges on the quartz crystal, causing its resonant frequency to change as the mass accumulates. By monitoring the crystal's resonant frequency over time, the rate of mass deposition can be calculated. QCMs offer direct mass flux measurements with excellent sensitivity, and they have been used extensively across the electrospray propulsion literature. For example, Thuppul et al. (2021) used a QCM to measure mass flux in the plume of a single capillary emitter spraying EMI-Im [15]. The resolution of QCM measurements can be improved by adding a QCM close to the first but shielded from incoming mass flux. The signal from the shielded QCM is subtracted from the main QCM signal to correct for the effects of ambient pressure and temperature and improve accuracy. In addition, active temperature control is sometimes used to further reduce thermal effects. This extension, sometimes called TQCM, has been used to achieve resolution roughly an order of magnitude higher than conventional QCM measurements. For example, Collins et al. (2022) used TQCM with a resolution of $2\ pg\ cm^{-2}s^{-1}$ to make mass flux measurements at high angles (> 30° half angle) in the plume of an EMI-Im capillary electrospray

source [16].

Quartz crystal microbalances have also been combined with retarding potential analyzers to conduct energy-dependent mass flux studies. Collins et al. (2022) used an RPA in tandem with a QCM to measure the mass flux in an EMI-Im capillary electrospray plume as a function of retarding potential [17]. At 'high beam currents' ($I_B = 610\ nA$), they found that neutral species accounted for more than 10% of the total mass flux. At 'low' beam currents ($I_B = 375\ nA$ and $I_B = 480\ nA$), neutral species accounted for less than 2% of the total mass flux. They also noted that the neutral mass fraction depends on angle and is highest at relatively high angles (~25° off axis) for the 610 nA beam. In another study, Geiger et al. (2022) used a QCM to measure mass flux in the plume of an externally wetted electrospray emitter spraying EMI-BF_4 [18]. They measured mass flux for four stopping potentials- 100 V, 300 V, 1300 V, and 2200 V. The only stopping potential that led to net positive mass flux measurements was 100 V, while QCM measurements for all other beam energies suggested net mass loss from the crystal surface. Their results pose critical questions for QCM measurements in electrospray plumes: *How much of the mass that impinges on the crystal actually stays there?* And *how much mass is removed from the crystal surface by plume bombardment?* These are questions being addressed by the growing field of electrospray plume – surface interactions, discussed briefly in section II.D.6. Despite their shortcomings, QCMs are one of the few direct measurement methods for plume mass flux. In contrast, *indirect* methods are sometimes used to estimate the plume mass flux from the current density and mass-to-charge distribution, as discussed in section III.

II.D.3. Stopping potential Distribution

The next fundamental plume property in our discussion is the *stopping potential,* sometimes called the *acceleration potential*. The stopping potential – literally the change in electrical potential required to stop a charged particle in motion – is the kinetic energy per charge of the particle expressed in terms of electrical potential (i.e., Volts). The stopping potential is related to the velocity of a particle by Eq. 1, where m is mass, q is charge, and $\zeta = (m/q)$ is the mass-to-charge ratio.

$$v = \sqrt{2\left(\frac{q}{m}\right)\phi_{SP}} = \sqrt{2\,\zeta^{-1}\,\phi_{SP}} \qquad \textbf{Eq. 1}$$

Commonly, stopping potential distributions are measured using electrostatic energy filters paired with a current detector, such as a Faraday cup. The trajectory of a charged particle through an electrostatic field depends only on the field strength and the particle's stopping potential. i.e., electrostatic fields do not separate particles by their mass or mass-to-charge. The simplest and most popular method for measuring stopping potential in electrospray plumes is the planar retarding potential analyzer (RPA), which usually consists of a set of conductive grids in front of a Faraday cup. The first grid (farthest from the cup) is usually held at ground potential, while the second grid is floated to the desired retarding potential. The RPA acts as a high pass filter, allowing particles with stopping potentials exceeding the retarding potential to pass through to the Faraday cup. By sweeping the retarding potential through the range of stopping potentials in the plume, the plume's stopping potential distribution can be measured.

Though the planar RPA is commonly used in electrospray propulsion, there are well-documented shortcomings of the design. Most importantly, the simple planar RPA has relatively poor resolution. The main cause of poor resolution in single-grid planar RPAs is that the RPA grid does not create a perfect isopotential surface. Instead, the retarding potential can 'sag' in the open areas in between grid wires. Enloe and Shell (1992) performed a case study and showed that the retarding potential can deviate from the applied potential (i.e., can 'sag') by up to 18% [19]. Their grids were relatively course, but their analysis shows that this effect can be significant. They provide analytical methods to calculate potential variation across an RPA grid given its geometry, and therefore to compute the expected resolution for a planar RPA. They propose improving the resolution of planar RPAs by increasing the number of retarding grids, thereby creating a more consistent retarding potential. In their case study, using a single RPA grid resulted in a maximum deviation in retarding potential of 18%, while the maximum deviation was only 0.7% for five RPA grids. The authors present computational and experimental results to demonstrate the improvement in RPA resolution using their method.

Later, a similar approach was used by Lozano (2006) to measure the stopping potential distribution in the plume of an externally wetted electrospray emitter spraying EMI-Im [20]. Another method for improving resolution is by using deflection-based electrostatic energy analyzers, such as an angled mirror [2] or more complex shapes [21].

Another significant source of error in planar RPA measurements is due to divergence of the plume. Planar RPAs filter particles by their axial velocity, i.e., the velocity component that is perpendicular to the grid. Therefore, particles entering the RPA at an angle are filtered out of the beam at a retarding potential that is lower than their actual stopping potential, which leads to error in the measured stopping potential. Lozano (2006) mitigated this problem by using an Einzel lens to focus the electrospray plume into a collimated beam, then using a multi-grid planar RPA to measure its stopping potential [20]. However, electrostatic focusing is only feasible for plumes that are nearly monoenergetic. Since the focusing properties of electrostatic lenses depend on stopping potential, focusing non-monoenergetic plumes introduces a *chromatic aberration* and distorts the measured potential distribution [22]. Other approaches to improve RPA resolution for off-axis particles include using curved RPA grids [23] and using a 'cup' shaped RPA rather than a planar grid design [24,25].

II.D.4. Mass-to-Charge Distribution

Electrospray plumes are made up of a diverse range of particles, which vary widely in their kinetic energy and mass-to-charge ratio. Therefore, each point in the plume has a distribution of stopping potential and mass-to-charge associated with it. The mass-to-charge distribution describes how the charge in the plume is distributed amongst the various plume species. For example, a capillary electrospray contains species ranging from polyatomic ions ($m/q \approx 10^2\ amu/q$) to charged nanodroplets ($m/q \approx 10^5\ or\ 10^6\ amu/q$). The class of instruments used to measure the mass-to-charge distribution are broadly called *mass spectrometers*. Perhaps the most common type of mass spectrometry used in electrospray propulsion is time-of-flight mass spectrometry (ToF-MS, or simply ToF). An example of a time-of-flight mass spectrometer is given in Figure 1, reproduced with permission from [3]. In ToF-MS, mass-to-charge is inferred from the flight time of the particles through a fixed distance. In other words, mass-to-charge is calculated from their velocities. In common electrospray propulsion experiments using ToF-MS, the plume is periodically interrupted using an electrostatic gate. When the plume is interrupted, the current measured by the ToF-MS collector decays to zero at a rate that is related to the flight time of particles in the plume. If the stopping potential is known, the mass-to-charge distribution can be computed from those flight times. ToF-MS has been used widely in the electrospray propulsion literature to study capillary [2,22,25,26], porous [9,27], and externally wetted [28] electrospray sources. There are other mass spectrometry techniques that have been applied to electrospray propulsion, such as quadrupole mass spectrometry [29]. However, the upper limit of mass-to-charge ratios that can be filtered by quadrupole mass filters is on the order of $10^3\ amu/q$, making them unsuitable for studying plumes that contain droplets in addition to ions and ion clusters.

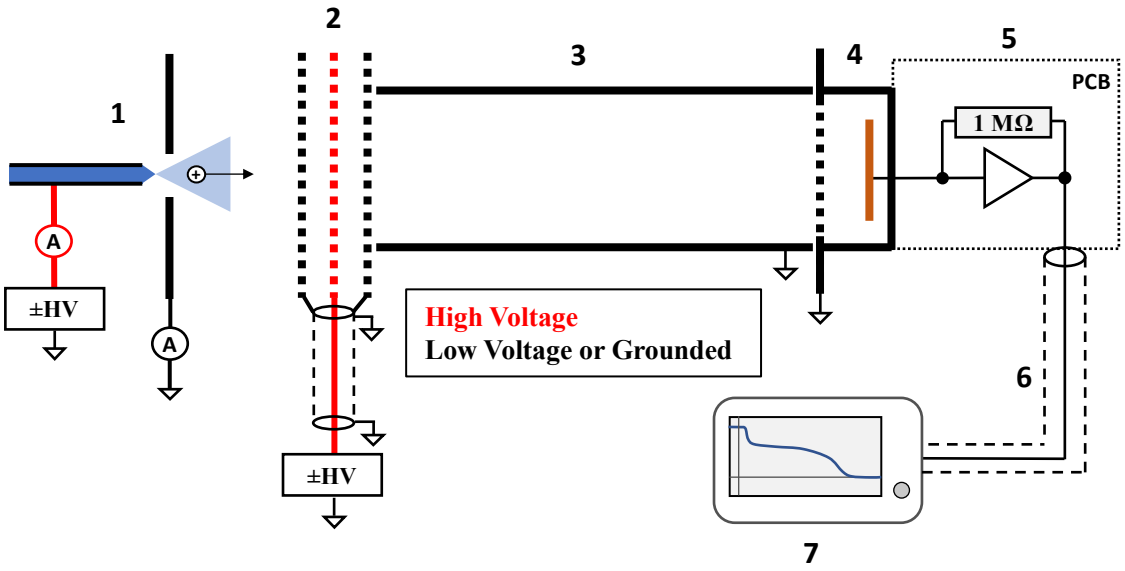

Figure 1: Time-of-Flight Mass Spectrometer (ToF-MS) from [3], reproduced with permission. (1) Electrospray source, (2) Electrostatic gate, (3) Drift tube, (4) Collector, (5) Transimpedance amplifier, (6) Coaxial cable, (7) Oscilloscope.

Perhaps the most compelling practical reason to measure mass-to-charge in an electrospray plume is to estimate the thrust and mass flow rate using plume data. This process is discussed in detail in section III. For now, we will simply say that it is possible, in principle, to calculate the flow rate and thrust by integrating the plume mass flux and momentum flux, respectively, over a surface enclosing the plume. The mass flux simply equals the charge flux (i.e., the current density) times the average mass-to-charge. However, the momentum flux can't be rigorously calculated using average values of stopping potential and mass-to-charge. Ideally, momentum flux would be calculated using a population distribution with stopping potential and mass-to-charge each as independent variables. To provide those data, mass spectrometry can be used in tandem with retarding potential analysis (RP/MS).

II.D.5. Tandem Measurements of Stopping potential and Mass-to-Charge

As discussed in the previous section, rigorously calculating the thrust from plume data requires that the population distribution of the plume be known as a function of mass-to-charge *and* stopping potential. For this application, mass spectrometry can be used in tandem with retarding potential analysis. Here, we abbreviate this approach as RP/MS (tandem Retarding Potential and Mass Spectrometry). There are several examples of RP/MS measurements in the electrospray propulsion literature, including RP with quadrupole mass spectrometry [30], RP with time-of-flight mass spectrometry [2,22,31], and orthogonal time-of-flight mass spectrometry [26,32], among others. However, most focus on the scientific value of RP/MS data rather than its application to indirect thrust measurement. For example, Gamero-Castaño et al. (2021) used RP/MS to study an EMI-Im capillary electrospray plume [2]. They used an angled mirror electrostatic RPA to direct species with the desired stopping potential into a time-of-flight mass spectrometer. Thus, mass-to-charge spectra were measured at specific stopping potentials. By sweeping the applied retarding potential through the range of stopping potentials in the plume, they measured mass-to-charge spectra for the full range of plume energies. Miller et al. (2021) used a similar technique, called orthogonal-acceleration time-of-flight (OA-ToF), for capillary electrosprays of four different propellants [26]. They presented their results in plots where both mass-to-charge and stopping potential are independent variables (see figure 3a in [26], for example). Both Gamero-Castaño et al. and Miller et al. used their data to determine the so-called 'jet breakup parameters', which are the velocity and electrical potential at which the jet emitted from the tip of the Taylor cone in capillary electrosprays breaks up into discrete droplets. To date, the RP/MS data presented by Gamero-Castaño

et al. and Miller et al. are some of the most valuable data for improving our understanding of the physics of capillary electrospray emission.

II.D.6. Other Plume Measurements

So far, we have discussed how various plume properties (current density, mass flux, stopping potential distribution, and mass-to-charge distribution) have been measured in electrospray plumes, sometimes as a function of position. We have also discussed how tandem instruments can be used to measure mass-to-charge distribution as a function of stopping potential to obtain a two-dimensional population distribution $f(\zeta, \phi)$ that can be used to calculate the momentum flux throughout the plume. In this section, we will describe other plume diagnostics for electrospray propulsion that are less common but still relevant.

▷ *Image Charge Detector (ICD) for Mass and Charge Measurements of Individual Droplets*

The first instrument we will discuss in this context is the *Image Charge Detector* (ICD). An ICD is an instrument that measures the magnitude of a charge in proximity to a sensing electrode, without the charge contacting the electrode. Gamero-Castaño (2007) used an ICD with multiple sensing electrodes to measure the charge and velocity of individual nanodroplets in an EMI-Im capillary electrospray plume [33]. From those data, he estimated the droplet diameter and mass-to-charge by assuming a value for the stopping potential. Later, Gamero-Castaño (2009) used an ICD in tandem with a retarding potential analyzer [34]. The RPA was used to select a specific stopping potential for ICD measurements. This approach removed the uncertainty in stopping potential that exists when an ICD is used alone, and thereby allowed for the accurate calculation of the diameter and mass-to-charge of individual nanodroplets. As far as I am aware, these studies are the only two examples where the charge, mass, and diameter of individual nanodroplets was measured for a capillary electrospray using an ionic liquid propellant. One drawback of Gamero's ICD method is that the charge on an individual nanodroplet is extremely small. The charge detection limit for Gamero's instrument was approximately 100 times the charge of an electron ($\sim 10^{-17}\ C$), so only nanodroplets with a charge exceeding this threshold could be studied.

▷ *Secondary Species Emission from Surfaces Bombarded by Electrospray Plumes*

Another topic worth mentioning here is secondary species emission from surfaces bombarded by electrospray plumes. It is well known that ion beams with keV stopping potentials can cause sputtering and/or charge emission from surfaces. A review of the literature suggests that the yields from electrospray plume bombardment are larger than those from monatomic ions at similar stopping potentials. For example, Borrajo-Pelaez et al. (2015) studied sputtering of gallium nitride by EMI-Im nanodroplet impact at high stopping potentials [35]. For a stopping potential of 9.9 kV, they measured a sputtering yield of nearly 2.2 atoms per incident molecule. Others have shown that surfaces bombarded by electrospray plumes emit charged particles in addition to sputtered neutrals [13,14]. Unlike secondary electron emission, they found that charged particles of both polarities were emitted from bombarded surfaces.

Uchizono et al. (2022) used a secondary species emission (SSE) probe to measure the charge yields for an EMI-Im capillary electrospray plume impacting a fritted stainless steel surface [14]. The SSE probe worked by on a principle similar to a Faraday cup with a secondary electron suppression grid. Each charge yield measurement consisted of three separate beam current measurements. The first measurement was simply the beam current with the SSE grid grounded. The next two measurements were done with the SSE grid biased to a positive or negative voltage. When a large enough bias is applied to the SSE grid, secondary species with the same polarity as the bias voltage are repelled by the grid and return to the surface. Thus, the secondary species of that polarity are 'suppressed', and the current measurement represents only the incident plume current and the current due to SSE of the opposite polarity. The incident current, negative charge yield, and positive charge yield can be calculated when these three measurements are taken together (i.e., three independent measurements for three unknowns). Uchizono et al. found that, for a 260 nA beam at a stopping potential of 1.4 kV, the secondary charge yields were $\gamma^+ = 0.13$ and $\gamma^- = 0.07$ when measured at the center of the plume. The yields rise to $\gamma^+ = 0.26$ and $\gamma^- = 0.21$ at 2.8 kV stopping potential, and to $\gamma^+ = 0.36$ and $\gamma^- = 0.33$ at 3.8 kV stopping potential. In this context, the charge yield γ is the number of secondary charges

emitted per incident charge. These results show that experimentalists should expect significant charge yield (and secondary species yield, more broadly) when working with capillary electrospray plumes at typical stopping potentials ($\sim 2 - 3\ kV$).

The results of similar studies performed on ion-dominated electrospray plumes, such as those from porous or externally wetted sources, also show that significant SSE occurs. For example, Klosterman et al. (2021) studied secondary charge emission from a variety of surfaces in the plume of an externally wetted emitter spraying EMI-BF_4. For stopping potentials of ±1.5 to ±2.9 kV, their measured charge yields were $\gamma^+ = 0$ to 0.55 and $\gamma^- = 0$ to 0.75 for cation (positive ion) bombardment and $\gamma^+ = 0$ to 0.4 and $\gamma^- = 0.3$ to 1.3 for anion bombardment. These yields are significantly above the yields for nanodroplets reported by Uchizono et al. However, the surfaces used by Klosterman et al. had different porosity, materials, and surface preparations. Therefore, their results are not directly comparable. In any case, these two studies show that secondary charge yield from electrospray plumes can be a significant source of error, for example, in plume current measurements. Furthermore, they show that by simply taking current measurements with and without SSE suppression the true incident current can be calculated. In other words, SSE effects can be removed from beam current measurements. Perhaps, then, it should be considered a "best practice" in electrospray diagnostics to incorporate SSE correction into our standard procedure for beam current measurements.

II.D.7. Summary of Plume Measurements and Methods

Table 1 summarizes the plume properties and plume diagnostic methods described in section II.D. The first column lists various quantities that can be measured when studying electrospray propulsion. These include system-level measurements (thrust and flow rate) as well as plume properties. The remaining columns each correspond to a diagnostic method. Cells with an 'x' denote direct measurements, while 'o' denotes that indirect estimates can be made using data from that diagnostic. The bottom row lists the subjective complexity of implementing each diagnostic method, graded from * (least complex) to *** (most complex).

Table 1: Summary of diagnostics used to measure plume properties. 'x' denotes direct measurement, while 'o' denotes in indirect estimate.

	RPA	QCM	MS	ICD	RP/ MS	RP/ QCM	RP/ ICD
Estimates:							
Thrust			o	o	o		o
Mass Flow Rate		x	o				
Plume Properties:							
Mass Flux		x	o	o	o	x	o
Current Density	x		o	o	o		o
Mass-to-Charge			x	x	x		x
Stopping potential	x				x	x	x
Droplet Mass							o
Droplet Charge				x			x
Neutral Mass Flux						x	
Complexity:	*	*	**	***	**	**	***

Nomenclature:

RPA- Retarding Potential Analyzer (used to measure stopping potential)

QCM- Quartz Crystal Microbalance (used to measure mass flux)

MS- Mass Spectrometry (used to measure mass-to-charge)

ICD- Image Charge Detector (used to measure charge and mass of individual nanodroplets).

RP/MS- Tandem instrument combining a retarding potential analyzer and a mass spectrometer

RP/QCM- Tandem instrument combining a retarding potential analyzer and a quartz crystal microbalance

RP/ICD- Tandem instrument combining a retarding potential analyzer and an image charge detector

III. Indirect 'Measurements' from Plume Data

So far, we've mostly discussed direct measurement methods. That is, methods where the quantity of interest is directly measured, for example by using a load cell to measure thrust. We've also seen that those measurements can be difficult and may require specialized equipment. In this section, we will discuss ways of indirectly 'measuring' the thrust and mass flow rate from plume data. Of course, with these methods we are just estimating the thrust and mass flow rather than actually measuring them. Researchers should keep in mind the inherent uncertainty of indirect 'measurements', and should not conflate them with true, direct measurements of thrust and mass flow.

III.A. Theoretical Framework for Indirect Measurement of Thrust and Mass Flow

In principle, it is possible to calculate the propellant mass flow rate and thrust using a control volume approach (Figure 1). The flow rate (Q) can be found by integrating the plume mass flux (j_m) over a surface enclosing the entire plume (Eq. 1). Similarly, the thrust can be found by integrating the axial momentum flux (j_{p_z}) over a surface enclosing the plume (Eq. 2).

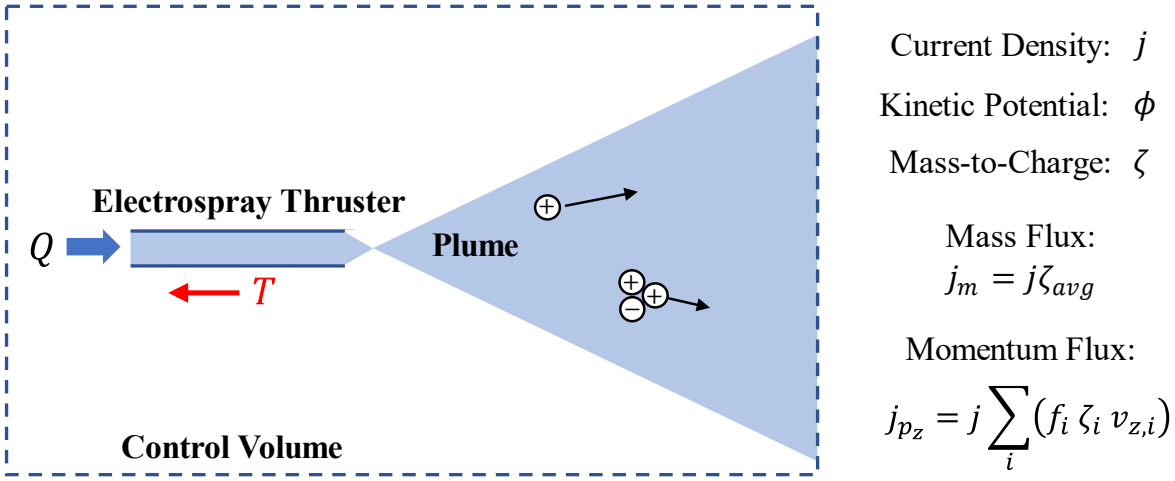

Figure 2: Control volume for an electrospray thruster.

$$\dot{m} = \int_A j_m \, dA \qquad \textbf{Eq. 2}$$

$$T = \int_A j_{p_z} \, dA \qquad \textbf{Eq. 3}$$

Let's first consider the plume mass flow. The mass flow through a surface element, dA, can be calculated from plume measurements by multiplying the charge flux (i.e., the current density) times the average mass-to-charge ratio (Eq. 4). The average mass-to-charge can be calculated using Eq. 5, where $f(\zeta)$ is the normalized population distribution in the plume. i.e., the integral of $f(\zeta)$ over $[0, \zeta_{max}]$ is one. Note that the current density j and the average mass-to-charge ζ_{avg} are functions of position, so evaluating Eq. 2 requires j and $f(\zeta)$ to be measured throughout the plume. While this is commonly done for current density (see [15], for example), measuring mass-to-charge at off-axis angles is less common. One notable exception is Lyne et al. (2022), who used ToF-MS to study the mass-to-charge distribution as a function of position in an EMI-Im capillary electrospray plume [3].

$$j_m = j\,\zeta_{avg} \qquad \textbf{Eq. 4}$$

$$\zeta_{avg} = \int_0^{\zeta_{max}} f(\zeta)\, \zeta\, d\zeta \qquad \textbf{Eq. 5}$$

Like mass flow, we find thrust by evaluating a surface integral of a flux. In this case, we use the axial momentum flux j_{p_z}. We can express j_{p_z} as the charge flux j times the average axial momentum per unit charge. For i particles in the plume, each with mass-to-charge ζ_i, axial velocity $v_{z,i}$, and current fraction f_i, the momentum flux is given by Eq. 6. The summation term represents the average axial momentum flux per charge, calculated as the average of the product $\zeta_i v_{z,i}$ weighted by f_i. Converted to an integral, the summation becomes Eq. 7.

$$j_{p_z} = j \sum_i \left(f_i\, \zeta_i\, v_{z,i}\right) \qquad \textbf{Eq. 6}$$

$$j_{p_z} = j \iint f(\zeta, \phi) \zeta v_z\, d\zeta\, d\phi \qquad \textbf{Eq. 7}$$

Unlike mass flow, the thrust cannot be rigorously calculated using average values for the mass-to-charge and the axial velocity. This is because the average of the product is not the product of the averages, i.e., $\sum f_i \zeta_i v_i \neq \zeta_{avg} v_{avg}$. Note that Eq. 7 uses $f(\zeta, \phi)$ while Eq. 6 uses $f(\zeta)$. This difference is significant: while $f(\zeta)$ can be measured simply using MS, $f(\zeta, \phi)$ *must* be measured using tandem RP/MS (see section II.D.5). Thus, mass flow rate can be estimated from standard plume data (j, RPA, MS) using Eq. 1 and Eq. 3. Thrust can be estimated using Eq. 3 and Eq. 7, but this requires more complex plume data (j, RP/MS). A reasonable approximation for the integral in Eq. 7 is given by Eq. 8, where the velocity v has been written in terms of ϕ using Eq. 1.

$$j_{p_z} = j \iint f(\zeta, \phi) \zeta v_z\, d\zeta\, d\phi \approx j \zeta_{avg} \cos\theta \sqrt{2\, \phi_{SP,avg}\, \zeta_{avg}^{-1}} \qquad \textbf{Eq. 8}$$

Note that the population distribution functions are normalized so that their integrals equal one. These normalization conditions are given in the following expressions. Also note that, due to these normalization conditions, the units of $f(\zeta)$ are $[kg/C]^{-1}$ and the units of $f(\zeta, \phi)$ are $[kg/C]^{-1}[V]^{-1}$.

$$\int_0^{\zeta_{max}} f(\zeta)\, d\zeta = 1$$

$$\int_0^{\phi_{max}} \int_0^{\zeta_{max}} f(\zeta, \phi)\, d\zeta\, d\phi = 1$$

III.B. Comparing Direct and Indirect Measurements

In this section, we discuss studies that compare estimates of thrust and flow rate to direct measurements. The estimates that we describe are derived from plume measurements of the current density, mass-to-charge distribution, and stopping potential distribution.

III.B.1. Ionic Liquid Ion Sources: Thrust

Courtney et al. (2016) is an excellent example of indirect thrust measurement using standalone RP and MS measurements [9]. They estimated thrust and flow rate for a porous electrospray thruster using ToF-MS and angle resolved current measurements. They assumed that the plume was monoenergetic and could be characterized by a single energy deficit (i.e., emitter potential minus stopping potential). They found that the effects of fragmentation were small (3%) and that the effect of energy deficit was also small. They accounted for losses due to beam spreading (i.e., cosine losses) by calculating an effective angle for their plume. They tested three thrusters, using an adapted mass balance for direct thrust measurements. For two of the three

thrusters, their estimates matched the direct thrust measurements. For the third thruster, direct measurements showed anomalous operation at high beam currents. The direct and indirect measurements differed by about 30% for the third source, while they agreed for the first two sources within ~10%. It's not clear why the direct and indirect measurements was larger for the third source, but one potential explanation is increased grid, causing the beam current to be significantly lower than expected. Another possible explanation is that a conductive path formed between the emitter and ground, causing the measured emitter current to increase. This could cause the indirect estimate to be too large, since it's assumed that all of the emitter current is contained in the plume. Whatever the cause, their results show that even careful attempts to indirectly 'measure' thrust are no replacement for direct measurements.

III.B.2. Capillary Electrosprays: Thrust

Unlike the porous electrospray thrusters used by Courtney et al., capillary sources typically have a wide stopping potential distribution (e.g., $\Delta\phi_{SP} = 500\,V$). So, stopping potential variation is like to have a significant effect on thrust for capillary thrusters. There are notable examples of direct thrust measurements of capillary electrospray thrusters in the literature [5,7]. Gamero-Castaño (2004) used a torsional thrust stand for direct thrust measurements of a six emitter capillary thruster [5]. He compared the direct measurements to thrust estimates obtained using ToF-MS and a constant 'representative' stopping potential. He found that the thrust estimated using ToF-MS data is about 15% lower than the direct thrust measurements. Several factors were considered to try and find the source of this discrepancy. First, Gamero used a large flat plate as the ToF-MS collector. Thus, the off-axis particles must travel farther than those on centerline to reach the collector, distorting the measured signal. However, as Gamero points out, this effect would tend to cause an overestimate of thrust using the ToF method. Instead, Gamero attributes this difference to the use of a single constant stopping potential (which he calls acceleration potential, V_a) and the magnitude of V_a that he chose to estimate the thrust.

Recent studies have shown that stopping potential is linearly related to average mass-to-charge in capillary electrospray plumes [2,26]. They show that high mass-to-charge droplets have the highest stopping potentials. Therefore, the mass weighted average stopping potential is higher than the charge weighted average. When estimating thrust (and mass flow, for that matter) using an average stopping potential weighted by mass is more accurate. In contrast, it is common practice to measure the plume's stopping potential distribution using a retarding potential analyzer, then compute the 'average' stopping potential from those data. However, the average stopping potential calculated from retarding potential data is weighted by charge rather than mass, and thus the average stopping potentials used in time-of-flight data analysis for capillary sources are often too low. Gamero goes on to point out [5] that "*A rigorous measurement of the thrust and mass flow rate based on the properties of the beam requires the spatial characterization of the velocity, specific charge and charge distributions of the beam*." This claim illustrates the challenges posed in evaluating Eq. 2 and Eq. 3. That is, the rigorous evaluation of thrust and mass flow require the distributions of velocity, specific charge, and charge at every point in the beam. Charge distribution is easily obtained from current density measurements. However, obtaining the velocity and mass-to-charge distribution requires either RP/MS data, or MS data paired with assumptions about the stopping potential. Furthermore, the former approach would require RP/MS data to be collected throughout the plume, which has not been done to date. Despite using several simplifying assumptions, Gamero demonstrated that thrust can be estimated for capillary electrospray thrusters using simple, plume-averaged data with an error of only 15%.

III.B.3. Ionic Liquid Ion Sources: Mass Flow

Natisin et al. (2021) investigated mass loss from a porous electrospray thruster operating with EMI-BF_4. They measured the plume-averaged stopping potential and mass-to-charge distributions using RPA and ToF-MS, respectively, and measured current density as a function of angle from the plume centerline. From those data, they estimated the propellant mass flow rate. They also took direct measurements of mass loss by weighing the thruster before and after the electrospray test. Comparing direct and indirect measurements shows that the mass flow rate during electrospray emission is nearly 2.7 times larger than mass loss estimates from ToF-MS. This is clearly a large error and has profound implications for the practical use of porous electrospray

thrusters in space. For example, they found that the average specific impulse demonstrated by their thruster was estimated to be 3831 s using the time-of-flight method, but only 1440 s when mass loss is measured directly. Another concern is investigating where the 'extra mass' is going since it does not appear to be present as charged particles in the plume. Extra mass that is emitted from the thruster has the potential to contaminate thruster components (e.g., extractor grids) or other spacecraft components. Several mass loss mechanisms were proposed, including propellant thermal or electrochemical decomposition, effects from high energy particle backstreaming, and undetected droplet emission. The main cause(s) of this anomalous mass loss are not known and require further study. Studies like this have led to a recognition that more direct mass loss measurements are needed to better understand ionic liquid ion sources and their potential for in-space propulsion. For example, Gilpin et al. (2022) recently presented a two-axis torsional thrust stand for simultaneously measuring thrust and mass loss during electrospray experiments. Through continued investigation, using plume measurements as one tool, our understanding of mass loss from ionic liquid ion sources can be improved.

III.B.4. Capillary Sources: Mass Flow

Studies comparing direct and indirect flow rate measurements for capillary electrospray thrusters [3,36] have generally shown better agreement than those reported for passively fed electrospray sources [1]. In general, passively fed sources hold propellant in a reservoir, and propellant moves to the emission site by capillary action. That is, the propellant is contained within the thruster and passively fed to the emitter tips. Flow rate is notoriously difficult to measure for passive thrusters, and often the only available means of flow rate measurement is by weighing the thruster before and after a test. In contrast, propellant is fed to capillary thrusters via tubing, often from an external propellant reservoir. One popular way to directly measure flow rate is to use transparent tubing (e.g., fused silica) and intentionally introduce a gas bubble into the feed tubing. By optically tracking the bubble and measuring its velocity, the flow rate can be calculated. Lyne et al. (2022) used this method to measure the flow rate for an EMI-Im capillary electrospray source [3]. They compared the direct measurements to estimates based on spatially resolved current density and ToF-MS data. Note that this is one of the few studies in the literature where ToF-MS is used to measure mass-to-charge distributions as a function of plume position, rather than simply using a plume-averaged mass-to-charge distribution. They found good agreement between indirect and direct mass flow measurements. The error for indirect estimates of mass flow was approximately 0 to 15%, with the indirect method tending to underestimate the true flow rate. Grustan-Gutierrez et al. (2017) reached a similar conclusion when comparing direct flow rate measurements with estimates based on time-of-flight data [36].

III.C. Best Practices for Indirect Estimates of Thrust and Flow Rate

To conclude this section, we recommend the following practices be adopted when estimating thrust and flow rate based on plume data:

1. For capillary electrospray thrusters, thrust and flow rate can be estimated from plume data with good accuracy (~15% in the studies discussed here). However, some assumptions about the stopping potential must be made if standalone RP and MS data are used rather than tandem RP/MS data. The stopping potential can be assumed to be constant (e.g., [5]), or linearly related to mass-to-charge (e.g., [3]). In any case, it is important that the assumptions made about the stopping potential are clearly stated whenever indirect measurements are reported, especially for time-of-flight data. For example, an author may write "*a constant stopping potential of* $\phi_{SP} = 1400\ V$ *was assumed for the calculation of thrust and propellant flow rate, and for time-of-flight data analysis*." Or "*a constant voltage deficit of* $\phi_E - \phi_{SP} = 100\ V$ *was assumed for all calculations*."

2. For ionic liquid ion sources (e.g., porous or externally wetted electrospray thrusters), indirect estimates are less accurate. Comparison of thrust estimates to direct estimates show that accurate estimates are possible if appropriate corrections are made [9]. However, those estimates cannot necessarily be considered reliable (see Figure 16a in [9], for example). Indirect estimates of flow rate for ionic liquid ion

sources should be considered unreliable in general. For example, Natisin et al. found that indirect estimates of flow rate for a porous electrospray thruster were about 2.5 times lower than direct measurements. Like capillary thruster results, authors should report what stopping potential was assumed in their data analysis.

IV. Summary

A variety of diagnostic techniques are used in electrospray propulsion research. This review has discussed some of these techniques for the measurement of thrust (II.B), propellant flow rate (II.C), and a variety of plume properties (II.D). Section III.A presented a theoretical framework for using plume data to estimate thrust and flow rate. And section III.B reviewed the literature for comparisons between direct measurements and those estimates. Finally, section III.C suggests 'best practices' for estimating thrust and flow rate from plume data.

Comparing direct and indirect measurements has demonstrated that the accuracy of plume-based thrust and flow rate estimates depends on the type of electrospray source (e.g., capillary, porous, etc.) and on the analysis methods used. For passively fed electrospray sources, Courtney et al. provide an excellent example of how thrust can be estimated indirectly. Their results suggest that it is possible to accurately estimate thrust if appropriate corrections are made. However, they also documented a large discrepancy between direct and indirect measurements for one of the three thrusters they tested. Others have documented large errors in flow rate estimates. For example, Natisin et al. found that their estimates of flow rate based on plume diagnostics differed from direct measurements by a factor of ~2.5. Taken together, these results suggest that thrust may be estimated indirectly with reasonable accuracy, but that indirect estimates of propellant flow rate should be considered unreliable for passively fed electrospray thrusters. For capillary thrusters, the story is simpler. A review of the literature suggests that thrust and propellant flow rate can be estimated from plume data with an accuracy of ~15%.

V. Acknowledgements

This work was supported by a NASA Space Technology Research Fellowship for Christopher Lyne, NASA Grant 80NSSC19K1165, with technical mentor Dr. Thomas Liu.

VI. References

[1] Natisin, M. R., Zamora, H. L., Holley, Z. A., Ivan Arnold, N., McGehee, W. A., Holmes, M. R., and Eckhardt, D. "Efficiency Mechanisms in Porous-Media Electrospray Thrusters." *Journal of Propulsion and Power*, Vol. 37, No. 5, 2021, pp. 650–659. https://doi.org/10.2514/1.b38160.

[2] Gamero-Castaño, M., and Cisquella-Serra, A. "Electrosprays of Highly Conducting Liquids: A Study of Droplet and Ion Emission Based on Retarding Potential and Time-of-Flight Spectrometry." *Physical Review Fluids*, Vol. 6, No. 1, 2021, p. 13701. https://doi.org/10.1103/PhysRevFluids.6.013701.

[3] Lyne, C. T., Liu, M. F., and Rovey, J. L. A Low-Cost Linear Time-of-Flight Mass Spectrometer for Electrospray Propulsion Diagnostics. 2022. IEPC-2022-178.

[4] De Borja De Saavedra, F., Wijnen, M., Correyero, S., Arboleya, G., and Pérez, D. Direct Thrust Measurements of an Externally Wetted Electrospray Thruster. 2022. IEPC-2022-223.

[5] Gamero-Castaño, M. "Characterization of a Six-Emitter Colloid Thruster Using a Torsional Balance." *Journal of Propulsion and Power*, Vol. 20, No. 4, 2004, pp. 736–741. https://doi.org/10.2514/1.2470.

[6] Gilpin, M. R., McGehee, W. A., Arnold, N. I., Natisin, M. R., and Holley, Z. A. "Dual-Axis Thrust Stand for the Direct Characterization of Electrospray Performance." *Review of Scientific Instruments*,

Vol. 93, No. 6, 2022. https://doi.org/10.1063/5.0087716.

[7] Demmons, N. R., Wood, Z., and Alvarez, N. "Characterization of a High Thrust, Pressure-Fed Electrospray Thruster for Precision Attitude Control Applications." *AIAA Propulsion and Energy Forum and Exposition, 2019*, No. August, 2019, pp. 1–15. https://doi.org/10.2514/6.2019-3817.

[8] Legge, R. S., and Lozano, P. C. "Electrospray Propulsion Based on Emitters Microfabricated in Porous Metals." *Journal of Propulsion and Power*, Vol. 27, No. 2, 2011, pp. 485–495. https://doi.org/10.2514/1.50037.

[9] Courtney, D. G., Dandavino, S., and Shea, H. "Comparing Direct and Indirect Thrust Measurements from Passively Fed Ionic Electrospray Thrusters." *Journal of Propulsion and Power*, Vol. 32, No. 2, 2016, pp. 392–407. https://doi.org/10.2514/1.B35836.

[10] Mier-Hicks, F., and Lozano, P. C. "Spacecraft-Charging Characteristics Induced by the Operation of Electrospray Thrusters." *Journal of Propulsion and Power*, Vol. 33, No. 2, 2017, pp. 456–467. https://doi.org/10.2514/1.B36292.

[11] Chakraborty, S., Courtney, D. G., and Shea, H. "A 10 NN Resolution Thrust-Stand for Micro-Propulsion Devices." *Review of Scientific Instruments*, Vol. 86, No. 11, 2015. https://doi.org/10.1063/1.4935471.

[12] Smith, K. L., Alexander, M. S., and Stark, J. P. W. "Voltage Effects on the Volumetric Flow Rate in Cone-Jet Mode Electrospraying." *Journal of Applied Physics*, Vol. 99, No. 6, 2006. https://doi.org/10.1063/1.2183351.

[13] Klosterman, M. R., Rovey, J. L., Levin, D. A., and Rao, A. "Ion-Induced Charge Emission from Unpolished Surfaces Bombarded by an [Emim][BF4] Electrospray Plume." *Journal of Applied Physics*, Vol. 131, No. 24, 2022. https://doi.org/10.1063/5.0060615.

[14] Uchizono, N. M., Marrese-Reading, C., Arestie, S. M., Collins, A. L., Ziemer, J. K., and Wirz, R. E. "Positive and Negative Secondary Species Emission Behavior for an Ionic Liquid Electrospray." *Applied Physics Letters*, Vol. 121, No. 7, 2022, p. 074103. https://doi.org/10.1063/5.0102592.

[15] Thuppul, A., Collins, A. L., Wright, P. L., Uchizono, N. M., and Wirz, R. E. "Mass Flux and Current Density Distributions of Electrospray Plumes." *Journal of Applied Physics*, Vol. 130, No. 10, 2021. https://doi.org/10.1063/5.0056761.

[16] Collins, A. L., Wright, P. L., Uchizono, N. M., and Wirz, R. E. High Angle Mass Flux of an Electrospray Plume. 2022. IEPC-2022-226.

[17] Collins, A. L., Wright, P. L., Uchizono, N. M., and Wirz, R. E. Neutral Mass Flux Measurements of an Electrospray Plume. 2022. IEPC-2022-227.

[18] Geiger, C. J., Bell, S., Chadwick, A., and Petro, E. M. Energy-Dependent QCM Measurements of an Electrospray Plume. 2022. IEPC-2022-221.

[19] Enloe, C. L., and Shell, J. R. "Optimizing the Energy Resolution of Planar Retarding Potential Analyzers." *Review of Scientific Instruments*, Vol. 63, No. 2, 1992, pp. 1788–1791. https://doi.org/10.1063/1.1143339.

[20] Lozano, P. C. "Energy Properties of an EMI-Im Ionic Liquid Ion Source." *Journal of Physics D: Applied Physics*, Vol. 39, No. 1, 2006, pp. 126–134. https://doi.org/10.1088/0022-3727/39/1/020.

[21] Collinson, G. A., Chornay, D. J., Glocer, A., Paschalidis, N., and Zesta, E. "A Hybrid Electrostatic

Retarding Potential Analyzer for the Measurement of Plasmas at Extremely High Energy Resolution." *Review of Scientific Instruments*, Vol. 89, No. 11, 2018. https://doi.org/10.1063/1.5048926.

[22] Lozano, P. C. *Studies on the Ion-Droplet Mixed Regime in Colloid Thrusters*. PhD dissertation, MIT, Department of Aeronautics and Astronautics, 2003. 29, 2003.

[23] Coles, T., Fedkiw, T., and Lozano, P. Investigating Ion Fragmentation in Electrospray Thruster Beams. In *48th AIAA/ASME/SAE/ASEE Joint Propulsion Conference & Exhibit*, American Institute of Aeronautics and Astronautics, 2012.

[24] Enloe, C. L. "High-Resolution Retarding Potential Analyzer." *Review of Scientific Instruments*, Vol. 65, No. 2, 1994, pp. 507–508. https://doi.org/10.1063/1.1145167.

[25] Gamero-Castaño, M. "Characterization of the Electrosprays of 1-Ethyl-3-Methylimidazolium Bis(Trifluoromethylsulfonyl) Imide in Vacuum." *Physics of Fluids*, Vol. 20, No. 3, 2008. https://doi.org/10.1063/1.2899658.

[26] Miller, S. W., Ulibarri-Sanchez, J. R., Prince, B. D., and Bemish, R. J. "Capillary Ionic Liquid Electrospray: Beam Compositional Analysis by Orthogonal Time-of-Flight Mass Spectrometry." *Journal of Fluid Mechanics*, Vol. 928, 2021, pp. 1–32. https://doi.org/10.1017/jfm.2021.783.

[27] Natisin, M. R., Zamora, H. L., McGehee, W. A., Arnold, N. I., Holley, Z. A., Holmes, M. R., and Eckhardt, D. "Fabrication and Characterization of a Fully Conventionally Machined, High-Performance Porous-Media Electrospray Thruster." *Journal of Micromechanics and Microengineering*, Vol. 30, No. 11, 2020, p. 115021. https://doi.org/10.1088/1361-6439/abb8c3.

[28] Gassend, B., Velasquez-Garcia, L. F., Akinwande, A. I., and Martinez-Sanchez, M. "A Microfabricated Planar Electrospray Array Ionic Liquid Ion Source With Integrated Extractor." *Journal of Microelectromechanical Systems*, Vol. 18, No. 3, 2009, pp. 679–694. https://doi.org/10.1109/JMEMS.2009.2015475.

[29] Miller, S. W., Prince, B. D., Bemish, R. J., and Rovey, J. L. "Electrospray of 1-Butyl-3-Methylimidazolium Dicyanamide Under Variable Flow Rate Operations." *Journal of Propulsion and Power*, Vol. 30, No. 6, 2014, pp. 1701–1710. https://doi.org/10.2514/1.B35170.

[30] Miller, S. W., Prince, B. D., and Rovey, J. L. "Capillary Extraction of the Ionic Liquid [Bmim][DCA] for Variable Flow Rate Operations." *48th AIAA/ASME/SAE/ASEE Joint Propulsion Conference and Exhibit 2012*, No. August, 2012, pp. 1–13. https://doi.org/10.2514/6.2012-3738.

[31] Gamero-Castaño, M. "Electric-Field-Induced Ion Evaporation from Dielectric Liquid." 2002, pp. 1–4. https://doi.org/10.1103/PhysRevLett.89.147602.

[32] Miller, S. W., Prince, B. D., and Bemish, R. J. "Orthogonal Time-of-Flight Mass Spectrometry of an Ion Beam with a Broad Kinetic Energy Profile." *Review of Scientific Instruments*, Vol. 88, No. 10, 2017. https://doi.org/10.1063/1.5007879.

[33] Gamero-Castaño, M. "Induction Charge Detector with Multiple Sensing Stages." *Review of Scientific Instruments*, Vol. 78, No. 4, 2007. https://doi.org/10.1063/1.2721408.

[34] Gamero-Castaño, M. "Retarding Potential and Induction Charge Detectors in Tandem for Measuring the Charge and Mass of Nanodroplets." *Review of Scientific Instruments*, Vol. 80, No. 5, 2009, pp. 1–5. https://doi.org/10.1063/1.3128730.

[35] Borrajo-Pelaez, R., and Gamero-Castaño, M. "Ultrafast Physical Sputtering of GaN by

Electrosprayed Nanodroplet Beams." *Materials Letters*, Vol. 159, 2015, pp. 110–113. https://doi.org/10.1016/j.matlet.2015.06.125.

[36] Grustan-Gutierrez, E., and Gamero-Castaño, M. "Microfabricated Electrospray Thruster Array with High Hydraulic Resistance Channels." *Journal of Propulsion and Power*, Vol. 33, No. 4, 2017, pp. 984–991. https://doi.org/10.2514/1.B36268.